Scientia Iranica F (2013) 20(6), 2323–2331

SCIENTIA
IRANICA

Sharif University of Technology
Scientia Iranica
Transaction F: Nanotechnology
www.scientiairanica.com

Doping assisted structural transition in copper substituted $MgFe_2O_4$ ferrite: Thermal, electrical and magnetic properties

S. Singhal[a,*], T. Namgyal[a], N. Laxhmi[b] and S. Bansal[c]

a. *Department of Chemistry, Panjab University, Chandigarh-160 014, India.*
b. *Department of Physics, M. L. Sukhadia University, Rajasthan, DST, New Delhi, India.*
c. *Department of Science and Technology, Technology Bhavan, New Mehrauli Road, New Delhi 110016*

Received 11 September 2012; received in revised form 23 April 2013; accepted 15 July 2013

KEYWORDS
Ferrites;
X-ray diffraction;
Electrical properties;
Saturation magnetization;
Coercivity.

Abstract. A cubic to tetragonal structure transition has evolved by substitution of Cu^{2+} ions in magnesium ferrite, fabricated via the sol-gel method. TEM studies revealed quasi-spherical particles for $MgFe_2O_4$ and rod-shaped particles for $CuFe_2O_4$, suggesting an enhancement of morphological anisotropy with Cu doping. Thermal analysis shows the formation of $MgFe_2O_4$ and $CuFe_2O_4$ at ∼380°C and ∼340°C, respectively, indicating a reduction in temperature for the formation of samples with copper doping. XRD shows the structural transition from a cubic to a tetragonal structure with increasing copper concentration. The dc electrical resistivity decreases with copper doping in $MgFe_2O_4$, attributing to the increase in conductivity due to Cu^{2+}-Cu^{+} ions hopping. $MgFe_2O_4$ has been found to have a saturation magnetization of ∼23 emu/g and a coercive field of ∼54 Oe. The saturation magnetization increases, while coercivity initially decreases and then increases with increasing copper concentration.

1. Introduction

Spinel structured nanoferrites have been a topic of research interest due to their vast applications in industrial, as well technological, areas. Magnesium ferrite, $MgFe_2O_4$, having a cubic structure, is a soft magnetic, *n*-type semiconducting material with applicability in a variety of fields, such as gas sensors, heterogeneous catalysis, microwave devices, magnetic cores, transformers, ferrofluids, etc. [1-5]. The superparamagnetism behavior of $MgFe_2O_4$ can also result in its use in bio medical applications [6]. Magnesium ferrite has also been reported to have high heat generation, as compared to other ferrites, when the grain size is in the μm range [7]. $MgFe_2O_4$ nanospheres prepared by Zhao et al. [8] have an excellent SO_2 absorption capacity for application in hot fuel gas desulfurization.

Magnesium ferrite has a general structural formula $[Mg_{1-x}Fe_x]^A[Mg_xFe_{2-x}]^BO_4$, where the square brackets, A and B, represent the cation occupancy of tetrahedral and octahedral sites, respectively. Therefore, cations such as Zn, Li, Cu, Mn, Ti, Ni etc. can be substituted in these sites to modify the properties of $MgFe_2O_4$. Kotnala et al. [9] studied the humidity sensing response of $Mg_{1-x}Li_xFe_2O_4$ $(0.0 \leq x \leq 0.6)$ prepared by a solid state reaction, and observed an enhanced sensitivity factor with Li doping. Ti-substituted magnesium ferrites were prepared by Purushotham et al. [10] to study the elastic behavior of the samples, and it was found that the elastic moduli first decreases and then increases thereafter. A double sintering technique was used by Kawade et

---

[*] *Corresponding author. Tel: +91-172-2534421*
E-mail address: sonal1174@gmail.com (S. Singhal)

al. [11] to synthesize Cr-substituted $MgFe_2O_4$ ferrites and a mechanism for the cation distribution of this spinel system using X-ray intensity calculations was reported. Copper has also been used as a dopant in magnesium ferrites, which resulted in the formation of ferrites at a low temperature. Substitution of copper also resulted in the enhancement of permeability as well as magnetization values, as suggested by Klug and Alexander [12]. The effect of Cu ions on the electromagnetic properties of MgZn ferrites was investigated by Rezlescu et al. [13], who found a decrease in d.c. resistivity and an increase in saturation magnetization with Cu^{2+} ion doping. The influence of copper ions in MgZn ferrites has also been studied by Reddy et al. [14], who observed an increase in initial permeability and dielectric constant and a decrease in dielectric loss with Cu doping for Mg. Copper ferrite is also found to have a spinel type fcc structure, as suggested by many authors [15-17], though they are found to be stable above 400°C. However, the tetragonal form has been found to be stable at room temperature only. The formation of the tetragonal form is due to the Jahn-Teller distortion effect, which leads to the formation of tetragonal copper ferrites at room temperature [18]. However, the cubic form exists as a metastable phase at room temperature.

Albeit many reports on the substitution of Cu in $MgFe_2O_4$, a systematic investigation of the structural transition with doping has not been made. The compositional level of copper as a dopant has also been found to be low. Therefore, in this study, the structural transition from cubic to tetragonal in $MgFe_2O_4$ maintaining a higher compositional level of copper substituent has been investigated. The simultaneous investigation of the electrical and magnetic properties of Mg ferrite with copper substitution has also been reported.

2. Experimental

2.1. Physical measurements

The infrared spectra were recorded using an FTIR instrument (PERKIN ELMER) for all the samples with KBr pellets between the range 4000-400 cm^{-1}. The X-ray diffraction studies were carried out using an X-ray diffractometer (Bruker AXS, D8 Advance) with CuKα radiation. TEM images were recorded using a Hitachi (H7500) Transmission Electron microscope, operated at 120 kV. The electrical properties were studied using a two probe method in the temperature range of 300-400 K. The powder samples were consolidated by applying a pressure of 5 tons to make a pellet of thickness 1-2 mm and diameter 12 mm. Silver paint was applied to both sides of the pellet, which was inserted between the probe and the base plate, and a constant voltage was applied. Corresponding current values were noted at different temperatures. The magnetic measurements were made on a Vibrating Sample Magnetometer (VSM) (155,PAR).

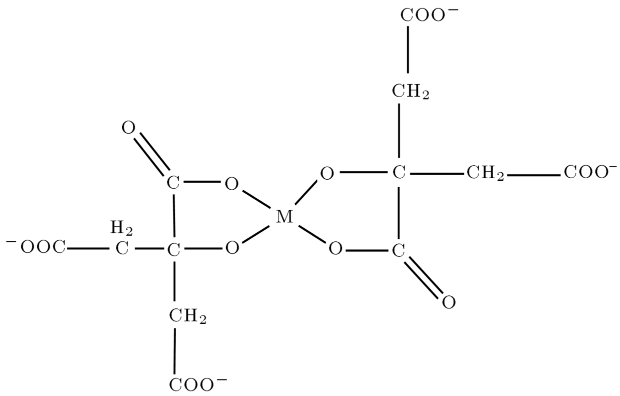

Figure 1. Chelation of the metal (M) ions with citric acid.

2.2. Preparation of $Mg_{1-x}Cu_xFe_2O_4$ ($0.0 \leq x \leq 1.0$) nanoferrites

The sol-gel method [19,20] has been used to induce a series of chemical reactions, including dissolution, hydrolysis, polymerization and decomposition, to obtain a homogeneous product at a low temperature. Analytical grade $Mg(NO_3)_2.6H_2O$ and $Cu(NO_3)_2.6H_2O$ have been used as starting materials for synthesizing $Mg_{1-x}Cu_xFe_2O_4$ ($0.0 \leq x \leq 1.0$) nanoferrites. The metal salts were dissolved in distilled water and citric acid was added to the metal salt solution in the molar ratio 1:1, as a chelating agent (Figure 1) for the homogeneous distribution of the metal salts. Ethylene glycol was then added which acts as a polymerizing agent in the reaction. The solution was stirred with continuous heating at 80-90°C, until gel formation, using a magnetic stirrer. Then, these gels were self ignited until ferrite powder was obtained, which was annealed at 400, 600, 800 and 1000°C for 2 h, for further characterization.

3. Results and discussions

3.1. FT-IR characterization

The FT-IR spectroscopy indicates the positions of the ions involved in the crystal lattice through their vibrational modes. The IR spectra of all the ferrites annealed at different temperatures show two fundamental peaks around 580-560 cm^{-1} and 450-430 cm^{-1} for all the annealed samples, which correspond to the crystal vibrations of M-O bonds in the ferrites. The frequency band near 580-560 cm^{-1} corresponds to the tetrahedral clusters and the band near 450-430 cm^{-1} corresponds to the formation of octahedral clusters [21]. The vibrational mode of tetrahedral clusters is higher compared to that of the octahedral clusters, because of the shorter bond length of Fe-O

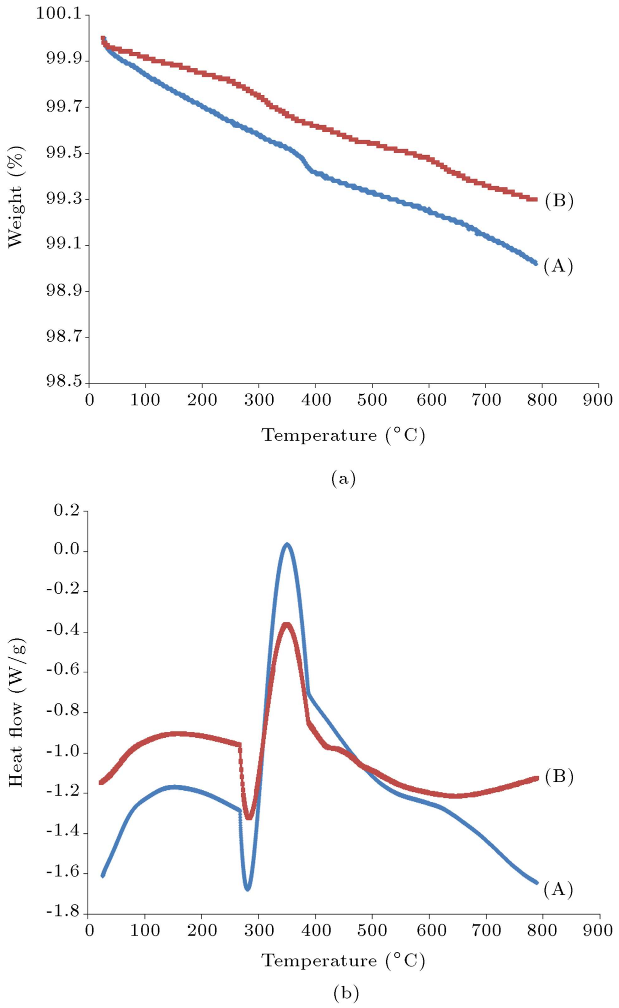

Figure 2. (a) TG curves and (b) DSC curves of the as obtained (A) $MgFe_2O_4$ and (B) $CuFe_2O_4$ nanoferrites.

distance (0.189 nm) in the tetrahedral sites compared to the Fe-O distance (0.199 nm) in the octahedral sites. It may be interpreted by the stronger bonding of Fe^{3+} ions at the A-sites rather than the B-sites.

3.2. Thermal analysis

Typical TG and DSC curves of, as obtained, $MgFe_2O_4$ and $CuFe_2O_4$ nanoferrites are shown in Figure 2(a) and (b) respectively. TG curves show that the formation of pure $MgFe_2O_4$ takes place at ~380°C and that of pure $CuFe_2O_4$ at ~340°C, suggesting a reduction in temperature for the formation of nanoferrites with Cu doping. The DSC curves show broad exothermic peaks at around 290°C in both cases. This is attributed to the decomposition of organic components left after the self-ignition method and combustion of the samples. The sharp endothermic peak at around 350°C, corresponding to a weight loss of about 1-2%, is attributed to the complete thermal decomposition of the samples and the formation of nanoferrites.

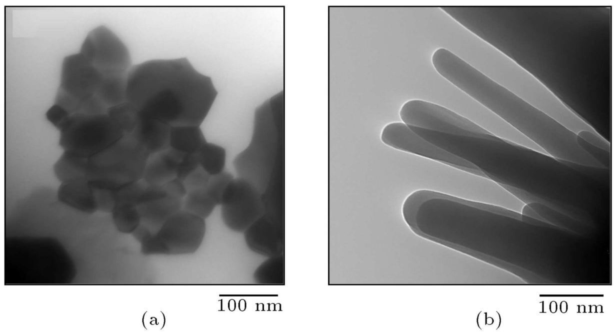

Figure 3. TEM images of (a) $MgFe_2O_4$ and (b) $CuFe_2O_4$ annealed at 1000°C.

3.3. Transmission Electron Microscope (TEM) analysis

TEM images have been recorded to investigate the grain size and morphology changes with copper doping. These images reveal that the particles of the, as obtained, samples are agglomerated and have spherical morphology with a particle size in the range 100-200 nm, similar to the results reported earlier [22]. This agglomeration may be attributed to the magnetic dipole interaction between the ferrite particles. However when the particles were agitated ultrasonically and taken onto a carbon grid, the particle size was observed to be ~ 10 nm, which increases with an increase in annealing temperatures. It is believed that the net decrease in the free energy of solid-solid and solid-vapour interface provides the necessary driving force for particle growth during the annealing process [23]. Figure 3(a) and (b) show the TEM images of $MgFe_2O_4$ and $CuFe_2O_4$, respectively, after annealing at 1000°C, having an uneven distribution of grain size. Interestingly, the morphologies in both cases have been observed to be different. $MgFe_2O_4$ nanoferrites have been found to be of a quasi-spherical shape, whereas $CuFe_2O_4$ nanoferrites have been observed to possess rod-shaped structures. Hence, an increase in morphology anisotropy has been observed with copper doping, which may be efficient for tuning the physical properties.

3.4. X-ray diffraction studies

A phase analysis for confirming the formation of the cubic and tetragonal structures has been done using powder X-ray diffractographs. Figure 4 shows the XRD pattern of $MgFe_2O_4$ nanoferrite samples annealed at different temperatures which reveals the formation of the single phased nanoferrite at 400°C. This suggests that these nanoferrites might have formed at a lower temperature, as discussed earlier in TG analysis. As the annealing temperature increases from 400 to 1000°C, the peaks grow sharper, attributing to an increase in particle size with increasing temperature, as suggested by Debye Scherrer [24]. XRD patterns of $Mg_{1-x}Cu_xFe_2O_4$ $(0.0 \leq x \leq 1.0)$ nanoferrites, after

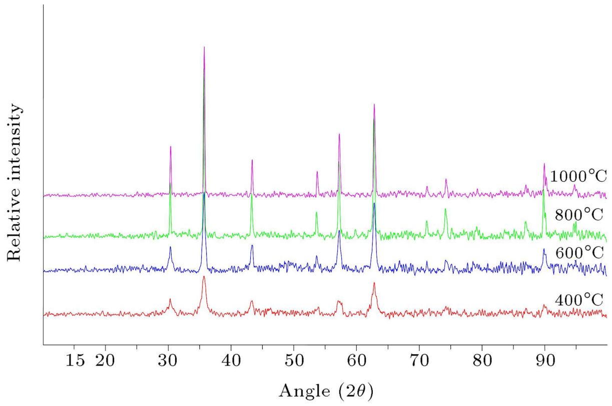

Figure 4. XRD patterns of $MgFe_2O_4$ nanoferrites annealed at different temperatures.

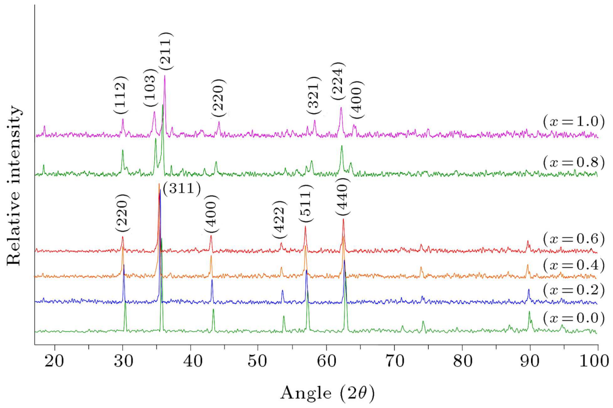

Figure 5. XRD patterns of $Mg_{1-x}Cu_xFe_2O_4$ ($x = 0.0$, 0.2, 0.4, 0.6, 0.8 and 1.0) annealed at 1000°C.

annealing at 1000°C, are shown in Figure 5, which indicate the cubic to tetragonal structure transformation. The peaks can be indexed to (220), (311), (400), (511) and (440) planes of the cubic unit cell up to the compositional level of copper having $x = 0.6$. For the copper compositional levels, $x = 0.8$ and $x = 1.0$, the XRD planes can be indexed to (101), (112), (103), (211), (220), (321), (224) and (400) planes, corresponding to the body centered tetragonal structure. The cubic phase has the space group Fd-3m and the body centered tetragonal has 141/amd as its space group. The Debye Scherrer equation has been used to calculate the crystallite size, considering the most intense peaks at the (311) plane for the spinel cubical structures and at the (211) plane for the tetragonal structures. The crystallite size of all the annealed samples at 1000°C is found to be in the range of 40-50 nm.

The dimensional changes in the lattice parameter have been calculated using Pawley and Le-Bail refinement methods and the results are found to be in accordance with Vegard's law. By a substitution of Mg^{2+} ions with Cu^{2+} ions, the lattice parameter does not show much change, attributing to the similar ionic radius of Mg^{2+} ion (72 pm) and Cu^{2+} ion (73 pm). The cubic structures have the lattice parameter 'a' around ∼8.375 Å, whereas the tetragonal structure has been found to exhibit the lattice parameters 'a' and 'c' values around 5.844 Å and 8.630 Å, respectively.

3.5. Electrical properties

The conductance in ferrites can be explained on the basis of the Verwey mechanism, which involves electron exchange between the ions of the same element present in more than one valence state, distributed randomly on equivalent lattice sites [25,26]. Ferrites structurally form a cubic close packed oxygen lattice, with the metal cations in tetrahedral (A) sites and octahedral (B) sites. The distance between the metal cations in B sites is smaller, compared to their distance in A and B sites. This leads to greater probability of electron hopping between the cations in B-B sites than A-B hopping. The probability of hopping in A-A sites is zero, because of which, A sites have only Fe^{3+} ions, and the Fe^{2+} ions formed occupy the B sites [27]. The conduction in ferrites is, therefore, due to the polaron hopping between Fe^{3+}-Fe^{2+} ions in the B sites. Therefore, the Fe^{3+}-Fe^{2+} ions hopping is responsible for the conduction in $MgFe_2O_4$ nanoferrite. However, with copper doping, the conductivity increases, which may be due to the additional effect arising from Cu^{2+}-Cu^{+} ions hopping. The equilibrium reaction existing in Mg-Cu nanoferrites is:

$$Cu^{2+} + Fe^{3+} \leftrightarrow Cu^{+} + Fe^{2+}.$$

Therefore, the conduction mechanism in Mg-Cu nanoferrites takes place through the valence exchange between Fe^{3+}-Fe^{2+} ions and Cu^{2+} and Cu^{+} ions, as in accordance with the Verway mechanism.

Room temperature DC resistivity for all the samples ($Mg_{1-x}Cu_xFe_2O_4$ ($0.0 \leq x \leq 1.0$) annealed at 1000°C is given in Figure 6. It has been observed that the resistivity (ρ) decreases from $\sim 1.32 \times 10^{10}$ ohm m

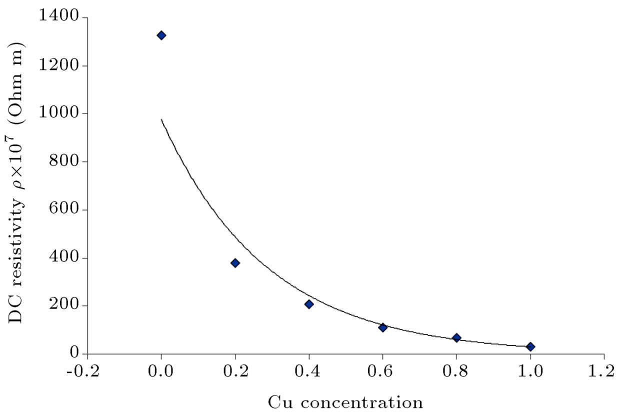

Figure 6. Variation of dc resistivity with copper concentration.

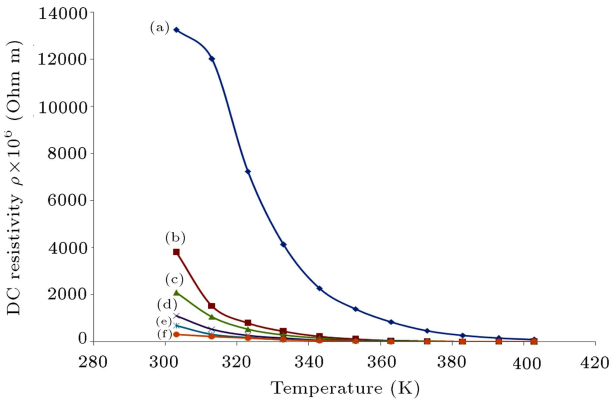

Figure 7. Temperature dependence of dc resistivity of $Mg_{1-x}Cu_xFe_2O_4$ with (a) $x = 0.0$, (b) $x = 0.2$, (c) $x = 0.4$, (d) $x = 0.6$, (e) $x = 0.8$ and (f) $x = 1.0$ nanoferrites annealed at 1000°C.

to $\sim 3.23\times10^8$ ohm m as the concentration of copper increases. This may be attributed to the increase in electron hopping between Cu^+-Cu^{2+} ions.

The temperature dependency of DC resistivity in the temperature range 313-373 K for all samples annealed at 1000°C is given in Figure 7. From this figure, it is observed that on increasing the temperature, resistivity decreases, due to the increasing hopping rates of electrons with temperature. This leads to activation of the electrons to jump from Fe^{3+} to Fe^{2+} and Cu^{2+} to Cu^+ ions in the B sites, showing the semiconductor behavior of the ferrite samples [28,29]. The activation energy (E_a) has been calculated using the Arrhenius type equation;

$$\rho = \rho_o \exp(E_a/kT),$$

where ρ_o is the resistivity at infinitely high temperature, k is the Boltzmann constant, E_a is the activation energy and T is the absolute temperature (in Kelvin). The slope of ($\log\rho$) versus ($1/kT$) gives the values of E_a values for all the samples and is shown in Figure 8. The value of activation energy for pure $MgFe_2O_4$ has been found to be ~2.75 eV. As the concentration of copper increases, the E_a first increases with initial doping of copper, then, it decreases beyond the compositional level of copper equal to $x = 0.2$.

The decrease in DC resistivity with increasing temperature leads to an increase in the drift mobility (μ) of the charge carriers. This is due to the thermal activation of the charge carriers with increasing temperature. The drift mobility (μ) of the charge carriers has been calculated using the equation:

$$\mu = (1/ne\rho),$$

where e is the electronic charge, n is the number of charge carriers and ρ is the DC resistivity at temperature T. The variation of drift mobility with resistivity

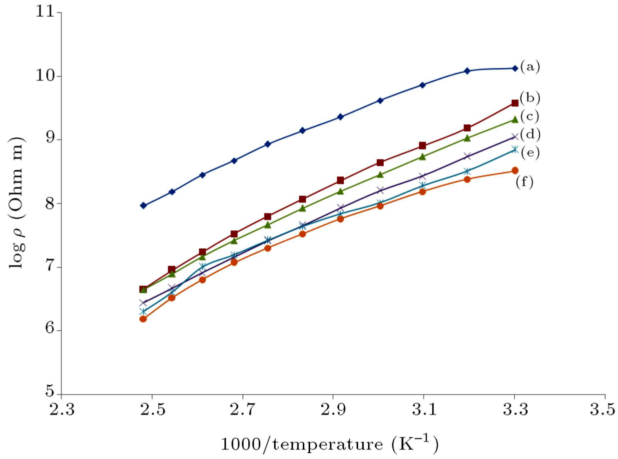

Figure 8. Arrhenius plots of $Mg_{1-x}Cu_xFe_2O_4$ with (a) $x = 0.0$, (b) $x = 0.2$, (c) $x = 0.4$, (d) $x = 0.6$, (e) $x = 0.8$ and (f) $x = 1.0$ nanoferrites annealed at 1000°C.

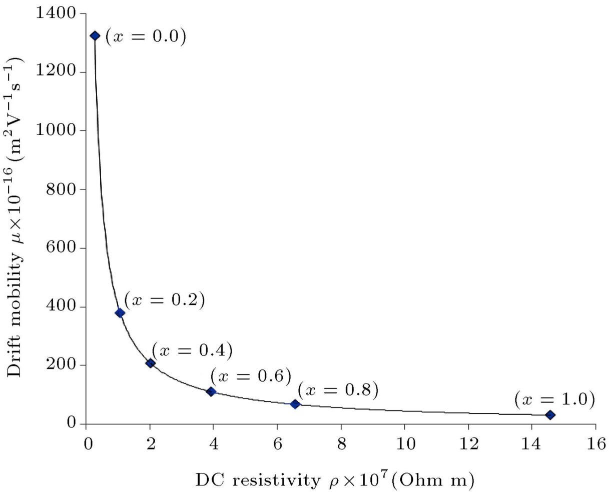

Figure 9. Variation of drift mobility v.s. dc resistivity at 313 K of $Mg_{1-x}Cu_xFe_2O_4$ ($0.0 \leq x \leq 0.0$) nanoferrites annealed at 1000°C.

at 313 K is shown in Figure 9, which shows that the samples having high resistivity have low mobility and vice versa. An increasing trend of drift mobility with increasing temperature was observed (Figure 10) due to the fact that the charge carriers started hopping from one site to another with increasing temperature [30]. The various electrical parameters are tabulated in Table 1.

3.6. Magnetic measurements

Magnetic hysteresis loops at room temperature for the annealed samples at 400, 600, 800 and 1000°C indicate an increasing trend of saturation magnetization with the annealing temperature, similar to the results reported earlier [31], which is due to the increase in particle size.

In the ferromagnetic spinels, the magnetic order is mainly due to the super exchange interaction

Table 1. Room temperature DC resistivity, drift mobility and activation energy of all the samples annealed at 1000°C.

Serial No.	Samples	DC Resistivity (ohm m)	Drift mobility ($m^2V^{-1}s^{-1}$)	Activation energy (eV)
1	$MgFe_2O_4$	1.325×10^{10}	2.972×10^{-17}	2.753
2	$Mg_{0.8}Cu_{0.2}Fe_2O_4$	3.801×10^{9}	1.077×10^{-16}	3.480
3	$Mg_{0.6}Cu_{0.4}Fe_2O_4$	2.087×10^{9}	2.035×10^{-16}	3.247
4	$Mg_{0.4}Cu_{0.6}Fe_2O_4$	1.118×10^{9}	3.932×10^{-16}	3.165
5	$Mg_{0.2}Cu_{0.8}Fe_2O_4$	6.932×10^{8}	6.576×10^{-16}	2.892
6	$CuFe_2O_4$	3.230×10^{8}	1.457×10^{-15}	2.800

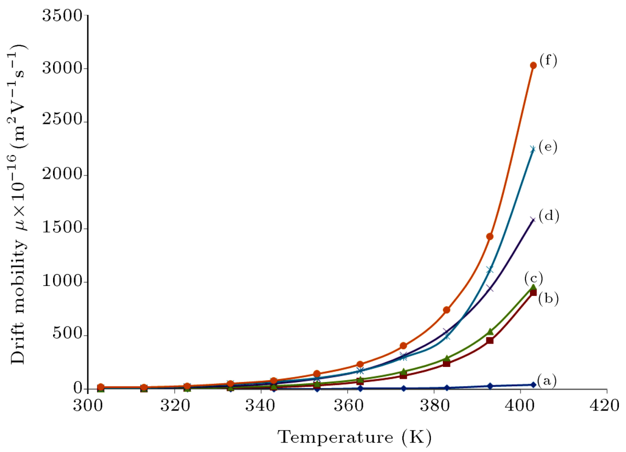

Figure 10. Temperature dependence of rift mobility of $Mg_{1-x}Cu_xFe_2O_4$ with (a) $x = 0.0$, (b) $x = 0.2$, (c) $x = 0.4$, (d) $x = 0.6$, (e) $x = 0.8$ and (f) $x = 1.0$ nanoferrites annealed at 1000°C.

Table 2. Saturation magnetization and Coercivity of all the samples annealed at 1000°C.

Serial No.	Sample	Saturation magnetization (emu/g)	Coercivity (Oe)
1	$MgFe_2O_4$	22.79	54
2	$Mg_{0.8}Cu_{0.2}Fe_2O_4$	24.95	30
3	$Mg_{0.6}Cu_{0.4}Fe_2O_4$	30.45	19
4	$Mg_{0.4}Cu_{0.6}Fe_2O_4$	33.88	57
5	$Mg_{0.2}Cu_{0.8}Fe_2O_4$	51.18	83
6	$CuFe_2O_4$	59.77	90

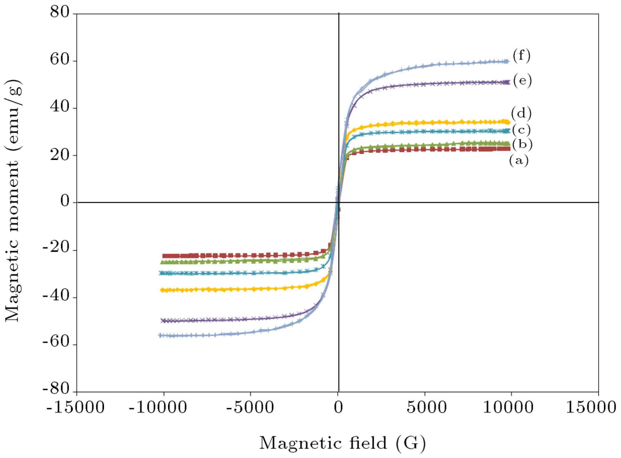

Figure 11. Hysteresis loops of $Mg_{1-x}Cu_xFe_2O_4$ with (a) $x = 0.0$, (b) $x = 0.2$, (c) $x = 0.4$, (d) $x = 0.6$, (e) $x = 0.8$ and (f) $x = 1.0$ nanoferrites annealed at 1000°C.

mechanism occurring between the metal ion in the *A* and *B* sublattices. $MgFe_2O_4$ possesses the fcc structure and has a magnetization value of ~23 emu/g. Various cations can be used as dopants to modify this magnetization value. Copper has been selected with the view that it results in enhancement of the magnetization values. In the present investigation, the M_s value increases up to ~60 emu/g, when Mg has been wholly replaced with Cu. The saturation magnetization and the coercivity of all the samples have been tabulated in Table 2. According to Neel's two sublattice model [32], the magnetic moment per formula unit in μ_B, $n_B^N(x)$ is expressed as:

$$n_B^N(x) = M_B(x) - M_A(x),$$

where M_B and M_A are the *B*- and *A*- sublattice magnetic moment in μ_B, respectively. $MgFe_2O_4$ has the general structural formula $[M_{1-x}Fe_x]^A[M_xFe_{2-x}]^BO_4$ (M = Mg), and the substitution of Cu^{2+} ion, having a preferential occupancy for the diamagnetic Mg^{2+} ion in the *B* site, thus, results in an increase of M_s value. Typical hysteresis loops of $Mg_{1-x}Cu_xFe_2O_4$ ($x = 0$, 0.2, 0.6, 0.8 and 1.0) nanoferrites annealed at 1000°C are shown in Figure 11, which shows that Cu substitution leads to a continuous increase in magnetization values. However, this increase is significant for higher Cu doped compositions. Initial copper substitution enhances the magnetization values to a lower extent, which may be due to the formation of Cu^+ ion in the cubic structures. Cu^+ has d^{10} configuration and, thus, the *d* orbitals are completely filled, which gives zero magnetic moment. At higher temperatures, there is a change in valence state from d^{10} to d^9, i.e., a monovalent to divalent transition of Cu ions. Cu^{2+} ion is a d^9 cation with *d* orbitals having an unpaired electron, thereby, contributing to

Table 3. Cation distribution of $Mg_{1-x}Cu_xFe_2O_4$ ($0.0 \leq x \leq 1.0$) nanoferrites annealed at 1000°C.

Composition (x)	Proposed cation distribution		Observed magnetic moment using Neel's model (BM)	Calculated magnetic moment (BM)
	A-site	B-site		
0.0	$(Mg_{0.08}Fe_{0.92})$	$[Mg_{0.92}Fe_{1.08}]$	0.80	0.81
0.2	$(Mg_{0.09}Fe_{0.91})$	$[Mg_{0.89}Cu_{0.02}Fe_{1.09}]$	0.91	0.92
0.4	$(Mg_{0.11}Fe_{0.89})$	$[Mg_{0.85}Cu_{0.04}Fe_{1.11}]$	1.14	1.17
0.6	$(Mg_{0.13}Fe_{0.87})$	$[Mg_{0.81}Cu_{0.06}Fe_{1.13}]$	1.36	1.36
0.8	$(Mg_{0.13}Fe_{0.87})$	$[Mg_{0.79}Cu_{0.08}Fe_{1.13}]$	2.10	2.12
1.0	$(Cu_{0.20}Fe_{0.80})$	$[Cu_{0.80}Fe_{1.20}]$	2.60	2.57

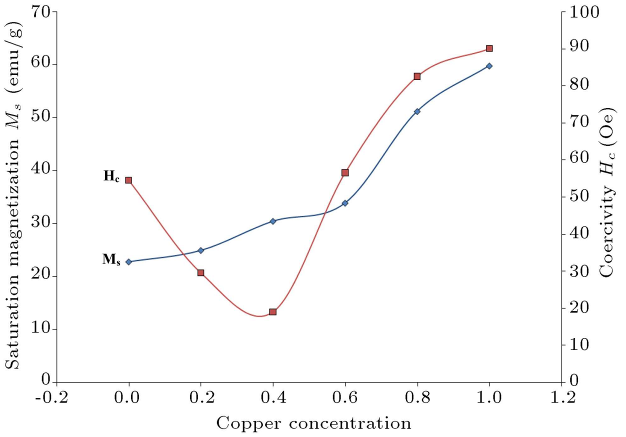

Figure 12. Variation of saturation magnetization (M_s) and coercivity (H_c) with copper concentration.

the magnetic moment. The sudden jump of M_s to high values with increased Cu concentration may be due to the preferential occupancy of Cu^{2+} in the B sites of a tetragonal structure. Therefore, the continuous increase in the M_s values with copper doping is due to the structural transition taking place with increasing Cu content (Figure 12). The structural transition results in the formation of a tetragonal structure, having whole M^{2+} ions in the octahedral sites. The structural transition leading to these magnetic changes is due to the Jahn Teller distortion effect [33], which is associated with the occupation of the Cu^{2+} ions in the B sites. Thus, Cu containing ferrites possesses unique structural modifications, which are absent in other mixed spinel systems.

The value of coercivity (H_c) initially decreases with copper doping, then it shows an increasing trend, as shown in Figure 12. This may be either due to an increase in grain size or an increase in morphology anisotropy, or both. This variation of H_c with grain size can be explained on the basis of domain structure, critical diameter and the anisotropy of the crystal [34,35]. In the single domain region, as the grain size decreases, the coercivity decreases, because of the thermal effects. The coercivity H_c in the single domain region is expressed as $H_c = g - h/D^2$, where g and h are constants. In the multi domain region, the variation of coercivity with grain size can be expressed as (in) $H_c = a + b/D$, where 'a' and 'b' are constants and 'D' is the diameter of the particle [36]. Hence, in the multi domain region, the coercivity decreases as the particle diameter increases. Moreover, the increasing trend of coercivity with increasing copper concentration may be attributed to the increase in anisotropy field, which in turn, increases the domain wall energy [37,38].

Cation distribution was obtained using the saturation magnetization per formula unit in the Bohr magneton for all the samples and is summarized in Table 3. The magnetic moment per unit per formula unit in the Bohr magneton (μ_B) has been calculated using the relation;

$$n_B = (M \times M_s)/5585,$$

where, M and M_s are the molecular mass and saturation magnetization, respectively. These calculated values were found to well obey those magnetic moments determined using Neel's model, as shown in Table 3.

4. Conclusion

$Mg_{1-x}Cu_xFe_2O_4$ (x = 0.0, 0.2, 0.4, 0.6, 0.8 and 1.0) nanoferrites have been prepared using the sol-gel method to investigate the effects of Cu-substitution on the structural, electrical and magnetic properties of $MgFe_2O_4$ nanoferrite. A structural transition from cubic to tetragonal form has been observed with the substitution of Cu^{2+} ions in magnesium ferrite. Thermal analysis shows that copper as a dopant can reduce the temperature of the nanoferrite formation. TEM images indicate semi-spherical shapes for $MgFe_2O_4$ nanoferrites and rod-shaped particles for $CuFe_2O_4$, which suggests an enhancement of morphological anisotropy with copper doping. The dc electrical resistivity decreases with copper doping in $MgFe_2O_4$, attributing to the increase in conductivity due to Cu^{2+}-Cu^{+} ions hopping. The activation energy first increases then decreases with Cu doping. The charge carriers start hopping from one site to another with increasing temperature, which results in an increase in drift mobility with temperature. $MgFe_2O_4$ has a saturation magnetization of ~23 emu/g, which shows an increasing trend with copper doping, having a maximum value of $M_s \sim 60$ emu/g for $CuFe_2O_4$. However, the coercivity initially decreases and finally shows an increasing trend, which may be attributed to the morphological transformations.

Acknowledgement

Financial support for this work under the UGC-major project scheme by UGC-New Delhi (India) is gratefully acknowledged.

References

1. Bharti, D.C., Mukherjee, K. and Majumder, S.B. "Wet chemical synthesis and gas sensing properties of magnesium zinc ferrite nano-particles", *Mater. Chem. Phys.*, **120**, pp. 509-517 (2010).
2. Lee, Y.H., Lee, G.D., Park, S.S. and Hong, S.S. "Catalytic removal of carbon particulates over $MgFe_2O_4$ catalysts", *React. Kinet. Catal. Lett.*, **84**, pp. 311-317 (2005).
3. Chen, Q., Rondinone, A.J., Chakoumakos, B.C. and Zhang, Z.J. "Synthesis of superparamagnetic $MgFe_2O_4$ nanoparticles by co-precipitation", *J. Magn. Magn. Mater.*, **194**, pp. 1-7 (1999).
4. Willey, R.J., Noirclerc, P. and Busca, G. "Preparation and characterization of magnesium chromite and magnesium ferrite aerogels", *Chem. Eng. Commun.*, **123**, pp. 1-16 (1993).
5. Van Uitert, L.G. "Magnesium-copper-manganese-aluminium ferrites for microwave applications", *J. Appl. Phys.*, **28**, pp. 320-322 (1957).
6. Chen, Q. and Zhang, Z.J. "Size-dependent superparamagnetic properties of $MgFe_2O_4$ spinel ferrite nanocrystallites", *Appl. Phys. Lett.*, **73**, pp. 3156-3158 (1998).
7. Maehara, T., Konishi, K., Kamimori, T., Aono, H., Hirazawa, H., Naohara, T., Nomura, S., Kikkawa, H., Watanabe Y. and Kawachi, K. "Selection of ferrite powder for thermal coagulation therapy with alternating magnetic field", *J. Mater. Sci.*, **40**, pp. 135-138 (2005).
8. Zhao, L., Li, X., Zhao, Q., Qu, Z., Yuan, D., Liu, S., Hu, X. and Chen, G. "Synthesis, characterization and adsorption performance of $MgFe_2O_4$ nanospheres for SO_2 removal", *J. Hazardous Mater.*, **184**, pp. 704-709 (2010).
9. Kotnala, R.K., Shah, J., Singh, B., Kishan, H., Singh, S., Dhawan, S.K. and Sengupta, A. "Humidity response of Li-substituted magnesium ferrite", *Sens. Actuators B*, **129**, pp. 909-914 (2008).
10. Purushotham, Y., Reddy, V.D., Reddy, M.B., Sagar, D.R., Kishan, P., Reddy, P.V. "Elastic behavior of titanium substituted magnesium ferrites", *Mater. Res. Bull.*, **30**, pp. 1015-1022 (1995).
11. Kawade, V.B., Bichile, G.K. and Jhadav, K.M. "X-ray and infrared studies of chromium substituted magnesium ferrites", *Mater. Lett.*, **42**, pp. 33-37 (2000).
12. Ghasemi, A., Ashrafizadeh, A., Jr, A.P., Machado, C.F.C., Shirsath, S.E., Liu, X. and Morisako, A. "The role of copper ions on the structural and magnetic characteristics of MgZn ferrite nanoparticles and thin films", *J. Magn. Magn. Mater.*, **322**, pp. 3064-3071 (2010).
13. Rezlescu, E., Sachelarie, L. and Rezlescu, N. "Influence of copper ions on the structural and electromagnetic properties of MgZn ferrite", *J. Optoelectron. Adv. Mater.*, **8**, pp. 1019-1022 (2006).
14. Reddy, M.P., Madhuri, W., Reddy, N.R., Reddy, K.V.S., Murthy, V.R.K. and Reddy, R.R. "Influence of copper substitution on magnetic and electrical properties of MgCuZn ferrite prepared by microwave sintering method", *Mater. Sci. Engg. C*, **30**, pp. 1094-1099 (2010).
15. Kester, E. and Gillot, B. "Cation distribution, thermodynamics and kinetics considerations in nanoscaled copper ferrite spinels. New experimental approach by XPS and new results both in the bulk and on the grain boundary", *J. Phys. Chem. Solids*, **59**, pp. 1259-1269 (1998).
16. Balaji, M., Raja, M.M., Asokan, K., Kanjilal, D., Rajasekaran, T.R. and Padiyan, D.P. "Effect of thermal spike energy created by $CuFe_2O_4$ by 150 MeV Ni11+ swift heavy ion irradiation", *Nuclear Instruments and Methods in Phys. Res. B*, **269**, pp. 1088-1091 (2011).
17. Lakhani, V.K. and Modi, K.B. "Al^{3+} modified elastic properties of copper ferrite", *Solid State Sci.*, **12**, pp. 2134-2143 (2010).
18. Lokhande, C.D., Kulkarni, S.S., Mane, R.S. and Han, S. "Copper ferrite thin films: Single-step non-aqueous growth and properties", *J. Crystal Growth*, **303**, pp. 387-390 (2007).
19. Singhal, S., Namgyal, T., Bansal, S. and Chandra, K. "Effect of Zn substitution on the magnetic properties of cobalt ferrite nanoparticles prepared via sol-gel route", *J. Electromag. Anal. Appl.*, **2**, pp. 376-381 (2010).
20. Lee, S.W., An, S.Y., Roon, S.R., Shim, I.-B. and Kim, C.S. "Atomic migration in $Co_{0.9}Zn_{0.1}Fe_2O_4$", *J. Magn. Magn. Mater.*, **254-255**, pp. 565-567 (2003).
21. Pradeep, A. and Chandrasekaran, G. "FT-IR study of Ni, Cu and Zn substituted nano-particles of $MgFe_2O_4$", *Mater. Lett.*, **60**, pp. 371-374 (2006).
22. Singhal, S., Baithwal, S.K. and Chandra, K. "XRD, magnetic and Mössbauer spectral studies of nano size aluminium substituted cobalt ferrites $CoAl_xFe_{2-x}O_4$)", *J. Magn. Magn. Mater.*, **306**, pp. 233-240 (2006).

23. Costa, A.C.F., Torella, E., Morelli, M.R., Neto, E.F. and Kiminami, R.H.G.A. "Investigation of sintered cobalt-zinc ferrite synthesized by co-precipitation at different temperatures: A relation between microstructure and hysteresis curves", *Mater. Res.*, **7**, pp. 523-528 (2004).
24. Klug, H.P. and Alexender, L.E., *X-Ray Diffraction Procedures for Polycrystalline and Amorphous Materials*, 2nd Edn., Wiley, Chapter 9 (1974).
25. Verwey, E.J.W., de Boer, F. and van Santen, J.H. "Cation arrangements in spinels", *J. Chem. Phys.*, **161**, pp. 1091-1092 (1948).
26. Verwey, E.J.W. and Haayman, P.W. "Electronic conductivity and transition point of magnetite Fe_3O_4)", *Physica*, **8**, pp. 979-987 (1941).
27. Hameda, O.M. and Barakat, M.M. "Effect of hopping rate and jump length of hopping electrons on the conductivity and dielectric properties of Co-Cd ferrite", *J. Magn. Magn. Mater.*, **223**, pp. 127-132 (2001).
28. Iqbal, M.J. and Siddiquah, M.R. "Structural, electrical and magnetic properties of Zr-Mg cobalt ferrite", *J. Magn. Magn. Mater.*, **320**, pp. 845-850 (2008).
29. Gabal, M.A. and Angari, Y.M.A. "Effect of diamagnetic substitution on the structural, magnetic and electrical properties of $NiFe_2O_4$", *Mater. Chem. Phys.*, **115**, pp. 578-584 (2009).
30. Islam, M.U., Chaudhry, M.A., Abbas, T. and Umar, M. "Temperature dependent electrical resistivity of Co-Zn-Fe-O system", *Mater. Chem. Phys.*, **48**, pp. 227-229 (1997).
31. Singhal, S. and Chandra, G.K. "Magnetic and Mössbauer spectral studies of nano crystalline cobalt substituted magnesium ferrites ($Mg_xCo_{1-x}Fe_2O_4$)", *Hyperfine Interactions*, **183**, pp. 75-80 (2008).
32. Neel, L. "Magnetic properties of ferrites: Ferromagnetism and anti-ferromagnetism", *Ann. Phys.*, **3**, pp. 137-198 (1948).
33. Krupichka, S. and Novak, P., *Oxide Spinels in Ferromagnetic Materials*, E.P. Wohlffarth., Ed., **3**, North Holland, Amsterdam, pp. 189-304 (1982).
34. Cullity, B.D., *Introduction to Magnetic Materials*, Addison-Wesely Publishing Company Inc., Reading MA (1972).
35. Chikazumi, S., *Physics of Magnetism*, Wiley New York (1959).
36. George, M., John, A.M., Nair, S.S., Joy, P.A. and Anantharaman, M.R. "Finite size effects on the structural, magnetic properties of sol-gel synthesized $NiFe_2O_4$ powders", *J. Magn. Magn. Mater.*, **302**, pp. 190-195 (2006).
37. Yakovlev, Y.M., Rubalikaya, E.V. and Lapovok, N. "Ferromagnetic resonance in lithium ferrite", *Sov. Phys.-Solid State*, **10**, pp. 2301-2303 (1969).
38. Jun, H.K., Koo, J.H. and Lee, T.J. "Study of Zn-Ti based H_2S removal sorbents promoted Co and Ni oxides", *Energy Fuels*, **18**, pp. 41-48 (2004).

Biographies

Sonal Singhal obtained her PhD degree in Chemistry, in 2003, from IIT Roorkee, India. She is currently Assistant Professor in the Department of Chemistry and Centre of Advanced Studies in Chemistry at Panjab University, Chandigarh, India. Dr. Singhal has more than 10 years of teaching experience, and has published/presented numerous papers in national and international journals and at conferences/symposia. Her research interests include synthesis and properties of nano size ferrites/oxides, formation of various types of nano composite materials and their magnetic properties and synthesis, and characterization of boron nitride nano tubes with different morphology and sizes and their applications.

Tsering Namgyal's biography was not available at the time publication.

N. Laxhmi's biography was not available at the time publication.

Sandeep Bansal obtained his PhD degree in Materials Sciences, in 2007, from IIT Roorkee, India, and is currently Scientist 'C' in the Department of Science and Technology in the Ministry of Sciences, New Delhi, India. Dr. Bansal has published/presented numerous papers in national and international journals and at conferences/symposia. His research interests include nano science and technology, and fracture mechanical studies of steel and materials selection.